A Decentralized Fault Section Location Method Using Autoencoder and Feature Fusion in Resonant Grounding Distribution Systems

Zi-Jing Li, *Graduate Student Member, IEEE,* Shuyue Lin, Mou-Fa Guo, *Member, IEEE,* and J. Tang

***Abstract*—In industrial application, the existing fault location methods of resonant grounding distribution systems suffer from low accuracy due to excessive dependence on communication, lack of field data, difficulty in artificial feature extraction and threshold setting, etc. To address these problems, this study proposes a decentralized fault section location method, which is implemented by the primary and secondary fusion intelligent switch (PSFIS) with two preloaded algorithms: autoencoder (AE) and backpropagation neural network. The relation between the transient zero-sequence current and the derivative of the transient zero-sequence voltage in each section is analyzed, and its features are extracted adaptively by using AE, without acquiring network parameters or setting thresholds. The current and voltage data are processed locally at PSFISs throughout the whole procedure, making it is insusceptible to communication failure or delay. The feasibility and effectiveness of the approach are investigated in PSCAD/EMTDC and real-time digital simulation system, which is then validated by field data. Compared with other methods, the experiment results indicate that the proposed method performs well in various scenarios with strong robustness to harsh on-site environment and roughness of data.**

***Index Terms*—Autoencoder (AE), backpropagation neural network, fault section location, resonant grounding (RG) distribution systems.**

I. Introduction

SINGLE phase to ground (SPG) faults are the most prevalent fault in resonant grounding (RG) distribution systems [1]. To avoid phase voltage rise and insulation degradation, it is of great necessity to identify and isolate SPG faults rapidly. Otherwise, it may cause two-point or even multi-point ground faults, thus critically threatening the system stability and power supply reliability [2]. Moreover, the existing fault indicators [3] in industry usually suffer from limited performances due to the communication failure and complex field environment, sometimes requiring the manual inspection to further confirm the fault point, which arouses wide concerns on the effectiveness of fault location in distribution systems.

The existing SPG fault location technologies can be roughly classified into three categories: signal injection method [4],[5], steady-state signal method [6],[7], and transient signal method [8]-[11]. As the limitations proposed in [8], the first two methods do not achieve satisfactory performances in RG distribution systems.

The transient zero-sequence signal is hardly influenced by the arc suppression coil (ASC) in the RG distribution system, so its features (such as amplitude, polarity, and energy characteristics) can be solely used for fault location. In [9], the energy of the transient zero-sequence current (TZSC) in the selected frequency band was utilized to locate the fault section. The test results indicated that it performed well under strong noise background and showed excellent robustness to variations in fault resistance, fault initial angle, line parameter, and load type. In [10], the amplitude information of TZSC was used to locate SPG faults by adopting edge computing with no requirement of precise synchronization. It had high accuracy in most of the fault conditions and was robust to measurement error and noise interference. However, the methods in [9] and [10] were susceptible to communication interference as massive data were needed to be transmitted from detection nodes to the distribution station or edge nodes. A protection scheme based on the similarity of TZSCs was proposed in [11] to locate the fault feeder. To identify the feeder type, a threshold was required to compare with the magnitude of grey relation degree. However, the selection of thresholds highly relies on the network structures and system parameters, which usually leads to poor universality.

Various algorithms have been used in literature to manually extract and analyze the features from transient signals, such as Hilbert-Huang transform [12], S-transform [13], mathematical morphology [14], etc. However, because the fault features are usually short and weak, methods that highly rely on artificially designed features are difficult to adapt to harsh field environment. With the development of machine learning techniques, adaptive feature extraction may offer a preferable solution. But many machine learning algorithms are dependent on massive training data, including the widely-applied convolutional neural network (CNN) [15],[16]. A fault location method based on the domain transformation with three-phase current and voltage signals was

Manuscript received May 22, 2021; revised October 6, 2021 and December 26, 2021; accepted February 5, 2022. This work was supported by the National Natural Science Foundation of China through the Project of Research of Flexible and Adaptive Arc-Suppression Method for Single-Phase Grounding Fault in Distribution Networks under Grant 51677030. (Correspondingauthors: Shuyue Lin; Mou-Fa Guo.)

Zi-Jing Li, Shuyue Lin, and Mou-Fa Guo are with the College of Electrical Engineering and Automation, Fuzhou University, Fuzhou 350108, China (e-mail: lizijing21@foxmail.com; shuyue.lin@fzu.edu.cn; gmf@fzu.edu.cn).

J.Tang is with the Shanghai Holystar In formation Technology Company, Ltd, Shanghai 200030, China (e-mail: tangj@holystar.com.cn).

Digital Object Identifier 10.1109/JSYST.2022.3151630

proposed in [16]. The six signals were transformed from time domain to image domain, and then the transformed images were processed by CNN. Although it worked well under various situations, a large amount of data was needed for training the location model. But the field fault data is not easily accessible, which results in the insufficient training, thus deteriorating the performance of fault location in the field. Therefore, in this study, autoencoder (AE) is adopted to reduce the nonlinear dimension of fault data effectively and extract optimal features adaptively without training, which can largely reduce the dependency of the subsequent classification algorithm on the amount of training samples and improve the working efficiency in various situations.

In most existing methods, massive data are required to be transferred from the feeder terminal units [17] to master station, which may lead to misidentification in case of communication error. Based on the primary and secondary fusion intelligent switch (PSFIS), a decentralized fault section locating method is proposed, which has the potential to solve the above problem. In this article, all the analyses are conducted at the PSFISs with the local data only, which can locally analyze fault data, identify section type and isolate fault section, with low communication requirements.

An AE and backpropagation neural network (BPNN)-based fault section location method is applied to detect SPG faults in RG distribution systems. The fault section can be identified by this approach via analyzing the relation between the TZSC and the derivative of the transient zero-sequence voltage (DTZSV). At each PSFIS, the features of TZSC and DTZSV are extracted adaptively by AE without training, and the section type is discriminated by BPNN. Finally, the fault section can be locally isolated by PSFIS. In the whole process, network parameters or manually-set thresholds are not required, so that the proposed method can be better adapted to various network structures and severe fault conditions in the field. In addition, it achieves decentralized fault locating and adaptive feature extraction with low communication burdens, which is more applicable to the harsh on-site environment.

The rest of the article is structured as follows. Section II explains the fault section location method in details. Section III expatiates the working principles of three compared methods. Section IV conducts simulations and experimental verifications. Finally, Section V concludes this article.

II. Fault Section Location Method

Once a permanent SPG fault occurs in the RG distribution system, the zero-sequence current (ZSC) and zero-sequence voltage are collected for the first half grid cycle by the PSFIS in each feeder section. Then, the DTZSV is obtained from the transient zero-sequence voltage (TZSV). After that, the two feature vectors are extracted adaptively from the normalized TZSC and DTZSV by using the AE network, which are then spliced to construct a characteristic vector (i.e. feature fusion). The first half of the characteristic vector is the current feature vector, and the second half is the voltage feature vector. Then, the characteristic vector is input into BPNN to identify whether the PSFIS is located at the upstream terminal of the fault point. If so, the PSFIS will wait for tripping according to a preset sequence defined by the ladder principle, which is a well-known rule to set the responding time delay [18] at switches in case of faults: the farther away from the power supply, the shorter the time delay is. Finally, the identification results will be uploaded to the master station, and the SPG fault will be locally isolated by the PSFIS with the shortest delay. Note that the BPNN is pretrained by a small amount of historical data. The framework of the proposed method is shown in Fig. 1.

A. Principle Analysis of Single Phase to Ground Faults

A group of positive-sequence current, negative-sequence current and zero-sequence current can be obtained by order component decomposition of the fault current at the fault point. The negative-sequence current only flows through the fault path after an SPG fault occurs, theoretically can be used for locating. Nevertheless, it is greatly affected by load current and other factors, which may lead to location failure. The ZSC is unaffected by load current, and it can be detected at all sections after an SPG fault occurs. Therefore, the existing fault location methods are mostly based on zero-sequence analysis.

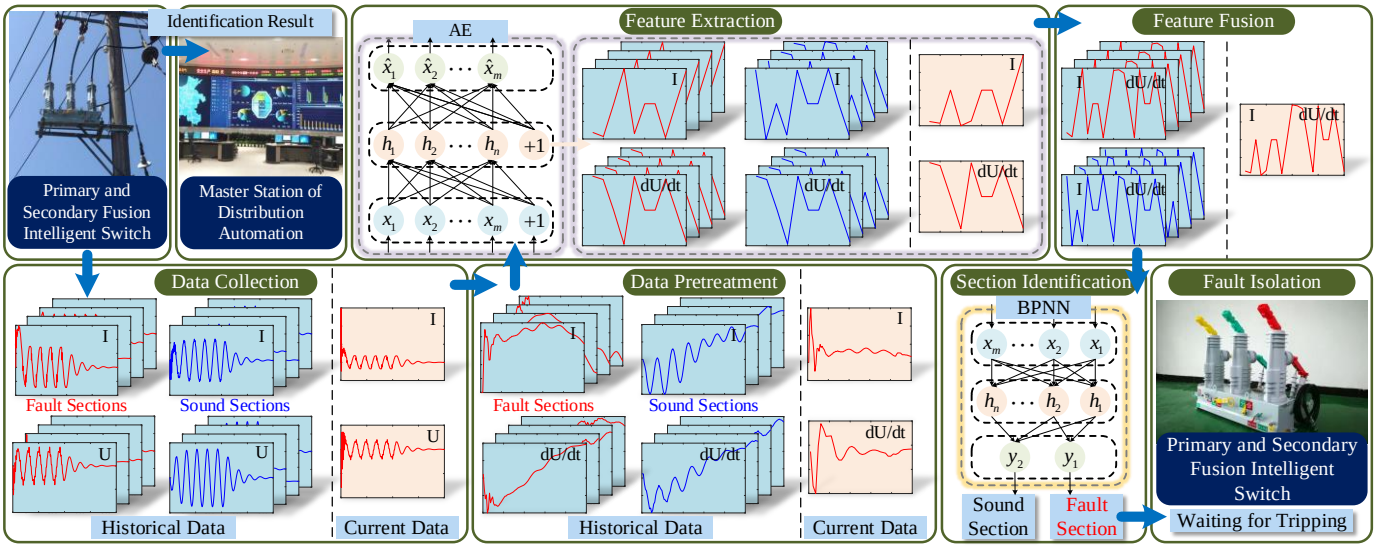

Fig. 1. Framework of the proposed method.

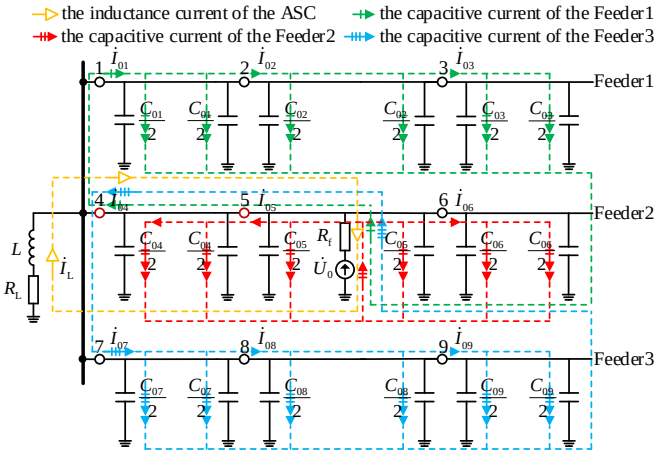

Fig. 2. Equivalent zero-sequence network diagram of SPG fault in the RG distribution system.

Fig. 2 shows the zero-sequence equivalent network of RG distribution system, the line series impedance and parallel conductance are ignored in this study. It is composed of three feeders with an SPG fault occurred in section-5. The feeders are divided into some feeder sections by detection nodes. And the number and location of detection nodes should be selected reasonably to optimize the reliability and economy of distribution system [19]. There are three detection nodes in each feeder in Fig. 2, which are numbered from 1 to 9. And the section number is defined as the nearest node number at its upstream terminal. In addition, the PSFISs are installed at detection nodes, with their numbers being the same as the corresponding nodes. In Fig. 2, C_{0i} is the zero-sequence distributed capacitance of section-*i*; L and R_{L} are the inductance and active loss resistance of ASC, respectively; R_{f} is the fault resistance; $\dot{U}_0$ is the voltage drop of virtual power supply at the point of fault; $\dot{I}_{0i}$ is the ZSC collected by the node-*i*; $\dot{I}_{\mathrm{L}}$ is the inductance current produced by the ASC.

In Fig. 2, the fault section refers to the section-5 where the fault point is located, and the section-4 in the upstream of fault point. Similarly, the sound section refers to the sections in sound feeders (i.e. section-1, 2, 3, 7, 8, 9), and the section-6 in the downstream of fault point.

In the fault sections (i.e. section-4, section-5), the relation between the TZSC and DTZSV is as follows:

$$i_{0i}(t) = -C_{1i}\frac{du_{0i}(t)}{dt} + i_{\mathrm{L}}(t)\,. \tag{1}$$

In the sound sections (i.e. section-1, 2, 3, 6, 7, 8, 9), the relation between the TZSC and DTZSV is as follows:

$$i_{0i}(t) = C_{2i}\frac{du_{0i}(t)}{dt} \tag{2}$$

where $i_{0i}(t)$ and $u_{0i}(t)$ are the TZSC and TZSV measured by PSFIS-*i*, respectively; $\dfrac{du_{0i}(t)}{dt}$ is DTZSV in PSFIS-*i*, obtained from TZSV; $i_{\mathrm{L}}(t)$ is the inductance current produced by ASC. C_{1i} is the sum of the capacitance of all sound feeders and the line between the PSFIS-*i* located at the upstream terminal of the fault point to the busbar; C_{2i} is the sum of the capacitance from the PSFIS-*i* located downstream of the fault point or at the sound feeder to the end of the feeder.

Moreover, for the sections located in the sound feeders (i.e. section-1, 2, 3, 7, 8, 9), the ZSC collected by the PSFISs can be expressed as follows:

$$\begin{cases} 3\dot{I}_{01} = \mathrm{j}3\omega\dot{U}_0\left(C_{01}+C_{02}+C_{03}\right) \\ 3\dot{I}_{02} = \mathrm{j}3\omega\dot{U}_0\left(C_{02}+C_{03}\right) \\ 3\dot{I}_{03} = \mathrm{j}3\omega\dot{U}_0 C_{03} \end{cases} \tag{3}$$

$$\begin{cases} 3\dot{I}_{07} = \mathrm{j}3\omega\dot{U}_0\left(C_{07}+C_{08}+C_{09}\right) \\ 3\dot{I}_{08} = \mathrm{j}3\omega\dot{U}_0\left(C_{08}+C_{09}\right) \\ 3\dot{I}_{09} = \mathrm{j}3\omega\dot{U}_0 C_{09}. \end{cases}$$

For the sections located in the fault feeder (i.e. section-4, 5, 6), the ZSC collected by the PSFISs can be expressed as follows:

$$\begin{cases} 3\dot{I}_{04} = -3\left(\dot{I}_{01}+\dot{I}_{07}-\dot{I}_{\mathrm{L}}\right) \\ 3\dot{I}_{05} = -3\left(\dot{I}_{01}+\dot{I}_{07}-\dot{I}_{\mathrm{L}}\right) - \mathrm{j}3\omega\dot{U}_0 C_{04} \\ 3\dot{I}_{06} = \mathrm{j}3\omega\dot{U}_0 C_{06}. \end{cases} \tag{4}$$

Therefore, the directions of ZSCs in each feeder are clearly indicated in Fig. 2. The current amplitude and direction in the fault section depend on the relationship between the inductor current and capacitor current. The steady-state zero-sequence current or voltage at the fault point will be suppressed to zero by the compensation effect of ASC, so as to extinguish the arc rapidly. But it inevitably leads to a large reduction in steady-state ZSC on fault path. In addition, the polarity of steady-state ZSC is the same in each section due to the overcompensation of ASC, and the directions are from the busbar to the feeder. As a result, in steady state, the fault features of overcompensation situation become too weak for location. As the inductance current of ASC can be ignored in the transient process due to its slow variation, the TZSC and DTZSV at the upstream node of fault point are opposite in polarity, while the polarity is the same amongst each other at other nodes. This above characteristic is used to identify whether the PSFIS locates in the upstream of the fault point. In addition, each PSFIS only needs to access its local data, which largely reduces the communication burden.

B. Acquisition of Characteristic Vector Based On AE

Currently, supervised-learning algorithms are widely applied to fault feature extraction in distribution systems, and require massive labelled training data. However, the field fault data is difficult to acquire, which results in insufficient training of supervised-learning algorithms and poor performances in the field. AE may provide a solution to improve the learning effect in case of small sample. It is an unsupervised-learning network, which can extract optimal features from unlabeled data adaptively and reduce nonlinear dimension effectively, thus contributing to an outstanding performance on site [20].

As shown in Fig. 3, AE is a three-layer network: input layer, hidden layer, and output layer. An activation function is required to activate the characteristics of neuron and map it out. The widely-used activation functions include sigmoid function, *tanh* function and *ReLU* function. Among them, only the *tanh*

function can map the data to the range of [−1,1]. Hence, the *tanh* function is used as the activation function in this study, which can better characterize the polarity features of fault information.

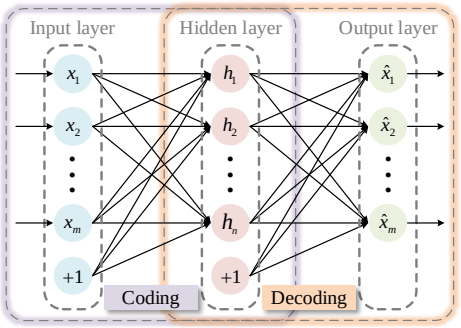

Fig. 3. Autoencoder structure.

The basic structure of AE is consisted of an encoder and a decoder. The encoder learns hidden features $\boldsymbol{h}$ from input data $\boldsymbol{x}$, which is called data dimension reduction. Then the decoder reconstructs the data with the learnt feature $\boldsymbol{h}$ to make the output data $\hat{\boldsymbol{x}}$ approximates $\boldsymbol{x}$. The encoding and decoding processes can be described as follows:

$$\boldsymbol{h}_i = \tanh(\boldsymbol{W}_i \boldsymbol{x} + \boldsymbol{b}_i) \tag{5}$$

$$\hat{\boldsymbol{x}}_j = \tanh(\boldsymbol{W}_j' \boldsymbol{h} + \boldsymbol{b}_j') \tag{6}$$

where i=1, 2, …, n; n is the number of neurons in hidden layer; j=1, 2, …, m; m is the number of neurons in output layer, which is equal to that in input layer; the $\boldsymbol{W}$ matrix is the coded weight parameter; the $\boldsymbol{W}'$ matrix is the decoded weight parameter; $\boldsymbol{b}$ is the coding bias vector; $\boldsymbol{b}'$ is the decoding bias vector.

To make $\hat{\boldsymbol{x}} \approx \boldsymbol{x}$, the error cost function is introduced in the training process. The objective function can be expressed as follows:

$$E = \frac{1}{2N}\sum_{i=1}^{N}\left\|\hat{\boldsymbol{x}}^{(i)} - \boldsymbol{x}^{(i)}\right\|^2 + \frac{1}{2}\lambda\left\|\boldsymbol{W}\right\|_2^2 \tag{7}$$

where N is the number of input data; λ is the weight attenuation parameter, $D = \frac{1}{2}\left\|\boldsymbol{W}\right\|_2^2$ is the weight attenuation term, both of them can reduce the weight.

After data collection, the data pretreatment is performed, including normalization. Its process can be described as follows:

$$\boldsymbol{X}_i^* = \frac{\boldsymbol{X}_i}{\max(|\boldsymbol{X}_1|, |\boldsymbol{X}_2|, ..., |\boldsymbol{X}_n|)} \tag{8}$$

where i=1, 2, …, n; n is the data points of $\boldsymbol{X}$; $\boldsymbol{X}$ is the original TZSC/DTZSV data; $\boldsymbol{X}_i$ and $\boldsymbol{X}_i^*$ are the ith data point of the original data and normalized data, respectively.

Then, the normalized TZSC and DTZSV are applied to AE for optimal feature vectors acquisition from the hidden layer. And the current and voltage feature vector are spliced to construct a characteristic vector. It is a good solution in lack of field fault data as there is no requirement for sample quantities. Moreover, the BPNN algorithm can have excellent performance without large training samples, making the proposed method have strong robustness to various conditions and harsh on-site environment.

C. Identification of Fault Section Based on BPNN

The structure of BPNN is similar to that of AE, which includes input layer, hidden layer, and output layer, as shown in Fig. 1. But the difference is that the number of neurons in the output layer of BPNN depends on the number of categories. BPNN has a simple computational structure with strong nonlinear mapping ability [21]. Therefore, the BPNN algorithm with two neurons in the output layer is used to discriminate section type in this article.

The learning process of BPNN can be divided into two steps, which are forward propagation and back propagation. BPNN is trained by the input data in the input layer and then processed by the function layer by layer. After that, by checking the final output with the expected value, the error signal will be detected and sent back to the input layer. The network connection weights are learned and adjusted through back propagation algorithm to reduce the error, which finally achieves successful mapping between given input and output.

The feature vectors of the current and voltage are extracted separately by AE and then spliced to generate a characteristic vector in each section. This characteristic vector is then identified by the pretrained BPNN to determine the section type. In this way, the fault data of each section is processed locally at the PSFIS of the respective section, which largely reduces the requirements for communication and improves the reliability of fault location.

D. Fault Isolation Based on the Primary and Secondary Fusion Intelligent Switch (PSFIS) in Distribution System

With the development of smart grids, rapid and local isolation to permanent SPG faults in RG distribution systems has become increasingly important. PSFIS is a device which is able to collect and analyze current/voltage data, so that it can isolate fault intelligently [22]. Thus, it may provide a potential carrier, whose structure is showed in Fig. 1, including current and voltage sensor, reclosing device, and control terminal.

As shown in Fig. 2, when a permanent SPG fault occurs in section-5, the PSFISs will collect the local fault data (the first half of grid cycle of the ZSC and ZSV after fault). Then, data analysis is conducted through the proposed AE-BPNN method to discriminate that the PSFIS locates in a fault section or a sound section. In this step, section-4 and section-5 are identified as fault section, respectively, while the rest are identified as sound section, respectively. Finally, the fault section will be isolated subjecting to the ladder principle. That is, PSFIS-5 will trip to realize the local isolation of the fault.

As defined in ladder principle, the responding delay of isolated action becomes longer as the fault occurs closer to the busbar. The delay time is generally set to millisecond level, and the inherent action time of PSFIS is about 30ms, which is within the acceptable range for RG distribution systems. In addition, if there are enough PSFISs to monitor the network, the suspected fault area where the SPG fault point is located will be shrunk as much as possible. But full coverage of detection equipment installation scheme has high investment costs [23]. Due to the tradeoff between reliability and economic concerns, only the feeder line with a high fault occurrence rate will be installed

with sufficient PSFISs. And the number of PSFISs will increase according to the fault occurrence probability. In this way, the areas that are more likely to fail can be fully covered by the detection units to quickly localized and isolated the fault through PSFISs in occurrence of a SPG fault [24].

The PSFISs upload identification results to the master station without sending massive fault data. Further analysis will be conducted at master station based on the network structure and these identification results. By deploying PSFISs in distribution networks, the proposed method is competent to realize rapid and decentralized SPG fault location and isolation without relying on communication and analysis of the master station.

III. Comparisons

To evaluate the performance of the proposed AE-BPNN method, three widely-applied fault location methods are studied for comparison in this article, including DTW-FCM algorithm (Method A), one-dimensional (1-D) CNN algorithm (Method B) and TZSC signal (Method C). Their working principles will be briefly illustrated in this section.

A. Method A: Based on DTW-FCM Algorithm

Fuzzy c-means (FCM) clustering is an effective pattern recognition method. Its feasibility to locate faults in distribution systems has been widely discussed in literature [25],[26]. For comparison, the improved dynamic time warping (DTW) together with the FCM are implemented to locate faults, which is entitled as Method A. See [25] for the principles of the improved DTW algorithm and FCM algorithm.

The implementation procedure is described in Fig. 4(a). First, PSFISs upload the collected ZSC data in the first half grid cycle after fault to master station. Next, the improved DTW is used to calculate the amplitude cross-correlation matrix (ACCM) of TZSC between two adjacent sections. Then, the comprehensive cross-correlation matrix (CCCM) is constructed via combining ACCM with the polarity cross-correlation matrix (PCCM) to indicate the amplitude and polarity information of TZSC. After that, FCM is applied to CCCM to distinguish the fault sections from sound sections. Finally, the section where has the fault is located by the master station through the topology structure, and a signal is generated to control the corresponding PSFIS to trip. This is a simple method without training or setting a threshold, however, it highly relies on uploading massive data to master station for fault identification.

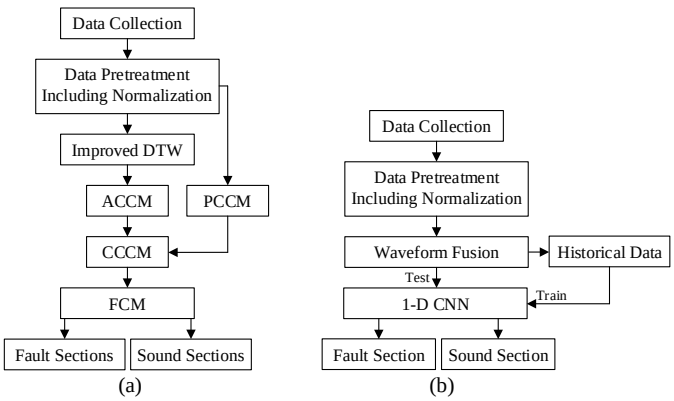

Fig. 4. Frameworks of the compared methods: (a) Method A; (b) Method B.

B. Method B: Based on 1-D CNN Algorithm

CNN shows great advantages on grounding fault location in comparison with traditional methods, as it extracts feature adaptively and achieves classification automatically. See [15] for the principle of 1-D CNN, and it is used to discriminate and isolate the fault section locally in this study for comparison. The ZSC and the derivative of zero-sequence voltage (DZSV) are normalized for first half grid cycle at PSFISs after faults. Then the normalized TZSC waveform and DTZSV waveform are spliced at each PSFIS (that is, waveform fusion). Then this 1-D spliced waveform is injected to 1-D CNN for fault section identification, as shown in Fig. 4(b).

C. Method C: Based on TZSC Signal

The similarity of TZSC waveforms between different feeder sections has been widely adopted for SPG fault location in RG distribution systems. Therefore, this transient signal is studied and compared with the proposed one. Firstly, the PSFISs upload the collected ZSC data in the first half grid cycle after fault to master station. After that, the AE is utilized to adaptively extract the feature vectors of TZSCs. Then, the two feature vectors of adjacent detection nodes are fused. And BPNN is applied to identify the fault sections from sound sections. Finally, the feeder section which has the SPG fault can be determined by master station through the distribution network structure. Method C does not require a voltage signal throughout the implementation process. But it relies on the high reliability of communication and the judgment ability of the master station.

IV. Simulation And Verification

In this section, the simulation and experiment validation are expatiated and analyzed in details, which includes simulation platform and model parameters, adaptability analysis based on the PSCAD/EMTDC simulation, adaptability analysis based on the real-time digital simulation (RTDS) data, and adaptability analysis based on the field data.

A. Simulation Platform and Model Parameters

PSCAD/EMTDC software is used to build a representative 10 kV RG distribution system model, which is often used in industrial applications, as shown in Fig. 5. The sampling frequency is set to 10 kHz and the sample points mentioned in this article refer to current/voltage data points collected by detection nodes. There are 18 PSFISs installed in the network, named F1-F18. The section number is defined as the detection node number at its upstream terminal, which is S1-S16. l_o is the length of the overhead line, l_c is the length of the cable line in km. The key parameters are specified in Table I.

It can be calculated that the sum of the grounded capacitance (C_Σ) in Fig. 5 is 7.584 μF. A generated arbitrary SPG fault drives the capacitive current exceeds the threshold at the fault point (I_C=41.2676A>20A). Therefore, an ASC is installed at neutral point according to the power system safety regulations. The overcompensation of the ASC is set to 5%, and its active power loss is set to be 3% of the inductive loss in this article. Accordingly, the equivalent inductance of ASC (L) is computed

to be 0.4241 H, the equivalent resistance (R_L) to be 3.9970 Ω.

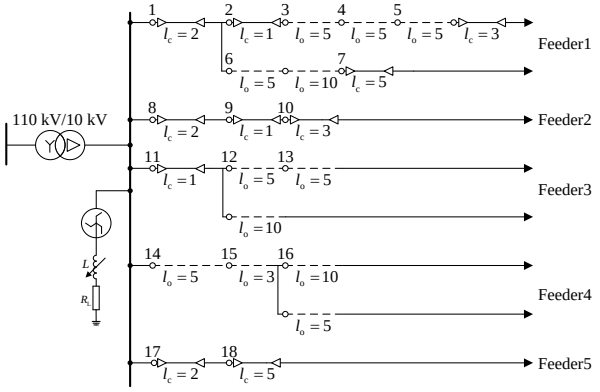

Fig. 5. 10 kV simulation model of RG distribution system.

TABLE I
PARAMETERS OF LINES

Type of Line	Sequence Components	Resistance (ohm/km)	Inductance (mH/km)	Capacitance (μF/km)
Cable Line	Positive Sequence	0.27	0.255	0.339
	Zero Sequence	2.7	1.019	0.28
Overhead Line	Positive Sequence	0.17	1.21	0.00969
	Zero Sequence	0.23	5.478	0.008

B. Adaptability Analysis Based on PSCAD/EMTDC Simulation

Using the described PSCAD/EMTDC simulation model in Fig. 5, SPG faults in phase A are simulated with different fault points (S_i), fault initial angles (θ) and fault resistances (R_f). The parameters of training samples and test samples are shown in Table II, which called typical fault. The training sample set and test sample set each contain 20 groups of fault cases, with fault data of 9 detection nodes in each group, making 180 groups of training samples and 180 groups of test samples in total.

The confusion matrix is employed to assess the performance of the proposed method and three compared methods. And the test results of typical fault are shown in Fig. 6 and Table III. Among them, Method A does not require training and has a fast running rate. Only the amplitude and polarity of TZSC are taken as the artificially designed clustering feature in this method, which results in a low reliability and low recognition accuracy of 85%. The accuracy of Method B is low (only 77.2%), which is mainly due to the discontinuity caused by the conjugation of the spliced waveforms. See Fig. 7 for the spliced waveforms for Method B. The first 100 data is the normalized TZSC, while the following 100 data is the normalized DTZSV. The last data of TZSC (the 100th point) may change arbitrarily in the range of [−1,1]. Hence, the change from the last current data (the 100th) to the first voltage data (the 101st) is drastic, which has a significant influence on the trend of splicing waveform. This increases the identification difficulties and leads to a poor F_1-score. If there are massive training samples to cover more possible cases, the performance of Method B will be improved.

In the proposed method, first, AE is used to extract the optimal feature vectors of TZSC and DTZSV, and then feature fusion is conducted. The last data of current feature vector (the 10th point in Fig. 9) is mostly 1, 0, or −1, which is in the same range of all the other data, making the conjugated characteristic vector a whole. Therefore, the subsequent classification algorithm BPNN is not affected by the conjunction of current and voltage, which results in the correct fault location in all 20 groups of typical fault cases.

TABLE II
TRAINING AND TEST SAMPLES OF SIMULATION DATA

Sample Type	S_i	θ (degree)	R_f (ohm)	Quantity
Training Sample	S_1-S_9	0,30,60,90	100,500,1000	180
Test Sample	S_8-S_{16}	10,45,70,85	300,700,900	180

TABLE III
PERFORMANCE OF THE PROPOSED METHOD AND COMPARED METHODS

Method	Accuracy	Precision	Recall	F_1-score
Proposed Method	100%	100%	100%	1
Method A	85.0%	69.4%	61.0%	0.649
Method B	77.2%	50.0%	29.3%	0.369
Method C	98.3%	97.5%	95.1%	0.963

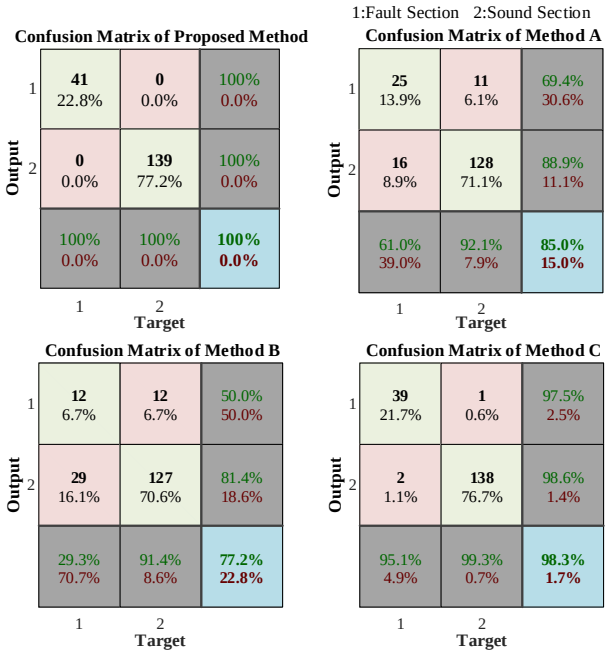

Fig. 6. Confusion matrixes of the proposed method and compared methods.

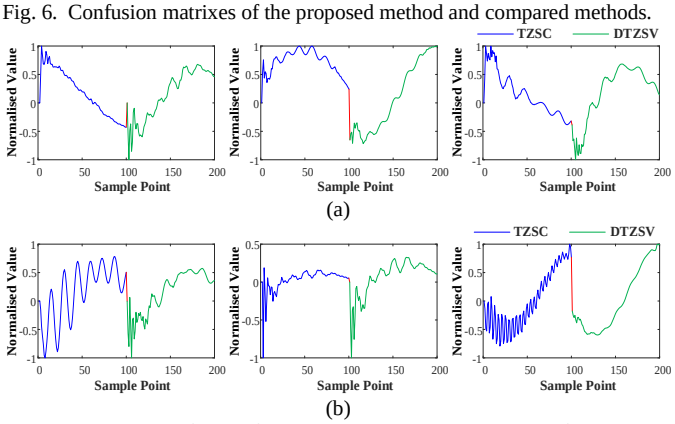

Fig. 7. Splicing waveforms of TZSC and DTZSV collected in (a) fault sections and (b) sound sections.

Some specific fault conditions are simulated in this article, including network structure changes (C1), fault occurs at the end of the feeder (C2), compensation degree changes (C3), and unsynchronized sampling (C4). These verification results (see Table IV) show that the proposed method based on AE-BPNN has the ability to accurately identify section types, even under severe working conditions. The Method A is greatly affected by the studied fault conditions, especially the unsynchronized sampling case with the F_1-score of only 0.357. The Method B

shows poor adaptability and low reliability with recognition rate less than 70%. Although Method C has good performance under most fault scenarios, it requires to transmit a large amount of current data. Since it is susceptible to the influence of communication quality, its reliability will have a downward tendency in practical application.

TABLE IV
TEST RESULTS OF SPECIFIC FAULT CONDITIONS

Fault	Method	Accuracy	Precision	Recall	F_1-score
C1	Proposed Method	100%	100%	100%	1
	Method A	85.7%	83.3%	71.4%	0.769
	Method B	68.3%	55.6%	23.8%	0.333
	Method C	100%	100%	100%	1
C2	Proposed Method	100%	100%	100%	1
	Method A	88.9%	91.7%	78.6%	0.846
	Method B	69.4%	61.5%	57.1%	0.592
	Method C	100%	100%	100%	1
C3	Proposed Method	100%	100%	100%	1
	Method A	100%	100%	100%	1
	Method B	66.7%	50.0%	33.3%	0.400
	Method C	100%	100%	100%	1
C4	Proposed Method	100%	100%	100%	1
	Method A	50.0%	31.3%	41.7%	0.357
	Method B	61.1%	37.5%	25.0%	0.300
	Method C	100%	100%	100%	1
C5	Proposed Method	97.2%	94.1%	100%	0.970
	Method A	83.3%	88.5%	71.9%	0.793
	Method B	59.7%	56.0%	43.8%	0.491
	Method C	83.3%	100.0%	62.5%	0.769
C6	Proposed Method	86.1%	89.3%	78.1%	0.833
	Method A	66.7%	64.3%	56.3%	0.600
	Method B	54.2%	47.6%	31.3%	0.377
	Method C	75.0%	76.9%	62.5%	0.690
C7	Proposed Method	94.4%	92.0%	95.8%	0.939

An exemplary fault (phase A, θ = 70°, R_f = 50Ω) occurs in S_9 in Fig. 5 to further illustrate the process of the proposed method. The fault data shown in Fig. 8 are collected by four PSFISs installed in F8-F11, respectively, where the SPG fault occurs at the 50th sample point. The ZSCs and DZSVs do not exist before the SPG fault occurs, but mutates after the fault. Hence, these two signals are utilized to implement decentralized fault section location. Specifically, the ZSC and DZSV in the first half grid cycle after fault are obtained at F8-F11. Each group of data contains 100 data points (50th point to 149th point). It can be seen from Fig. 8(b) that the DTZSVs in four PSFISs are similar, whereas the amplitude and polarity of the TZSCs collected at detection points (F8-F9 and F10-F11) are different. This is consistent with the principle of SPG fault in RG distribution systems analyzed above. Then, TZSC and DTZSV are normalized and fed into AE network to extract the feature vector, respectively. After that, feature fusion is conducted, in which the feature vectors of current and voltage are spliced to construct a characteristic vector in each section (see Fig. 9). Each contains 20 data points, where the first ten is the current feature vector, and the last ten is the voltage feature vector. It can be seen from Fig. 9 that the characteristic vectors at the upstream node of fault point are significantly different from vectors at the other nodes. Then, the spliced characteristic vector is fed into the trained BPNN to identify the section type. There is no need to set a threshold during the whole process. To achieve a good convergence performance, the number of hidden layer nodes in AE and BPNN are both set as 10 in this article.

C. Adaptability Analysis of High Impedance Fault and PSFIS Sampling Error

In an high impedance fault (HIF) generates somewhere, the amplitude of fault current is relatively small. Most fault section location methods are susceptible to this weak fault feature. Therefore, the Emanuel model [27] is used to generate HIFs for

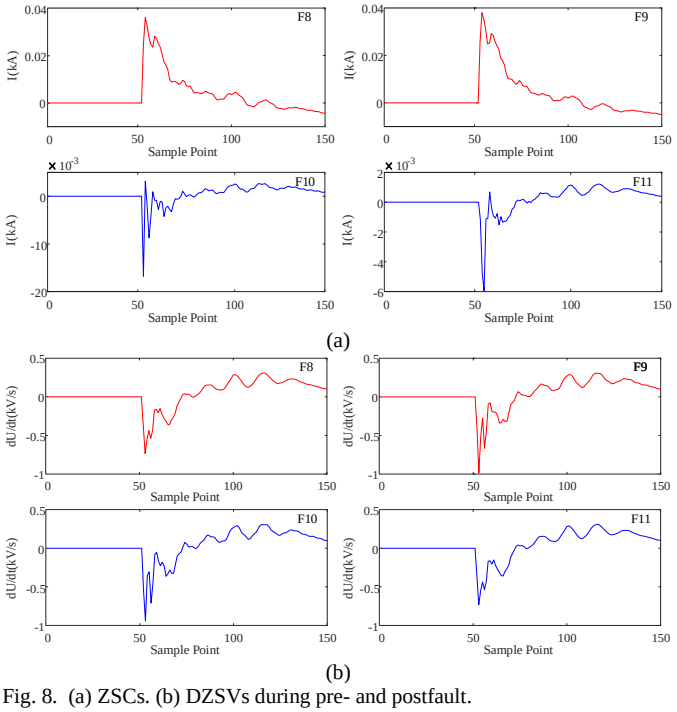

Fig. 8. (a) ZSCs. (b) DZSVs during pre- and postfault.

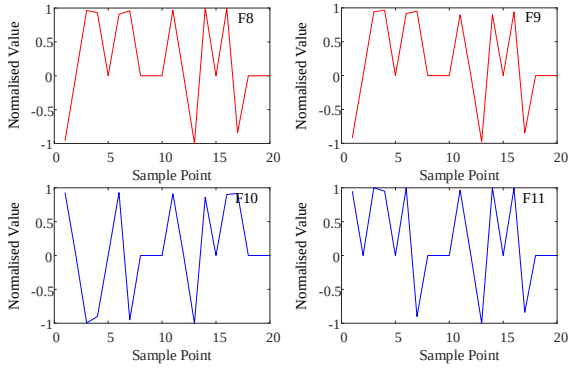

Fig. 9. Characteristic vector in each detection node.

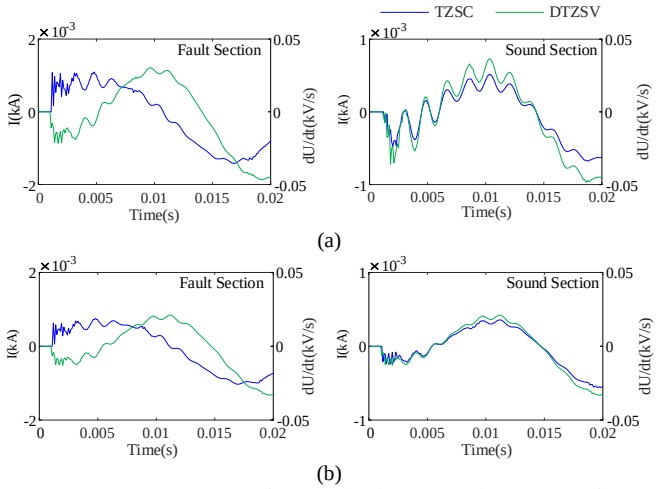

Fig. 10. TZSCs and DTZSVs of HIFs. (a) Rf = 2000 Ω, θ = 60°. (b) Rf = 3000 Ω, θ = 45°.

validating the proposed method. The HIFs with fault resistances of 2000 and 3000 Ω (C5) are simulated and the results are shown in Table IV. The proposed method has a high accuracy of 97.2%. The TZSC and DTZSV waveforms of HIFs are shown in Fig. 10. It can be seen that the TZSC and DTZSV of fault sections keep the opposite polarity during the initial stage after the fault occurs, while the polarity of the sound sections is always the same, which is sufficient for the method to accurately identify the fault section. However, the proposed method is susceptible to noise in HIF, as the F_1-score is 0.833 in the case of HIF accompanied by noise interference (15, 20dB) (C6). The sampling accuracy of PSFIS will also limit the accuracy of fault location method, especially after synthesis to zero sequence, this error will be further amplified. The combined effects of three-phase asynchronous sampling and the inaccurate sampling of amplitude are considered in this article. At this time, the polarity relationship is not destroyed, and the method shows a high accuracy and precision in PSFIS sampling error condition (C7).

D. Adaptability Analysis Based on RTDS Data

As the RTDS system shown in Fig. 11, eight PSFISs are installed in the network. About 12 groups of SPG fault are generated, including 48 sets of data. The sampling frequency is set to 10 kHz. See Table I for the parameters of lines. The TZSCs, DTZSVs, and spliced characteristic vectors of two fault sections and two sound sections are shown in Fig. 12. Significant differences in the fault and sound section characteristic vectors indicate the effective feature extraction of AE. As a result, the section types can be effectively discriminated by BPNN.

The RTDS data is used as an example to illustrate the sample coverage of the BPNN in this study due to the lack of field fault data. The parameters of the 12 fault cases are listed in Table V. Six of the fault cases are selected as training samples (25 sets of data in total) while the rest are test samples. The test accuracy shown in Table VI is only 82.6% with low reliability. That is because there are more samples of sound sections and fewer samples of fault sections, which makes the fault sections in test sample set difficult to be identified. Hence, the fault data with ten fault sections and ten sound sections are selected as training samples, which improves the test accuracy to 96.4%. Finally, the test results of the proposed method and the compared methods are shown in Table VII. The number of test data is 48 in Method A. And Method C is not tested due to the small amount of fault data.

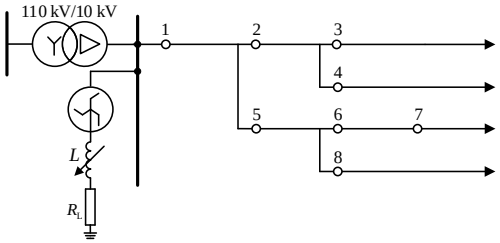

Fig. 11. Network structure of RTDS system.

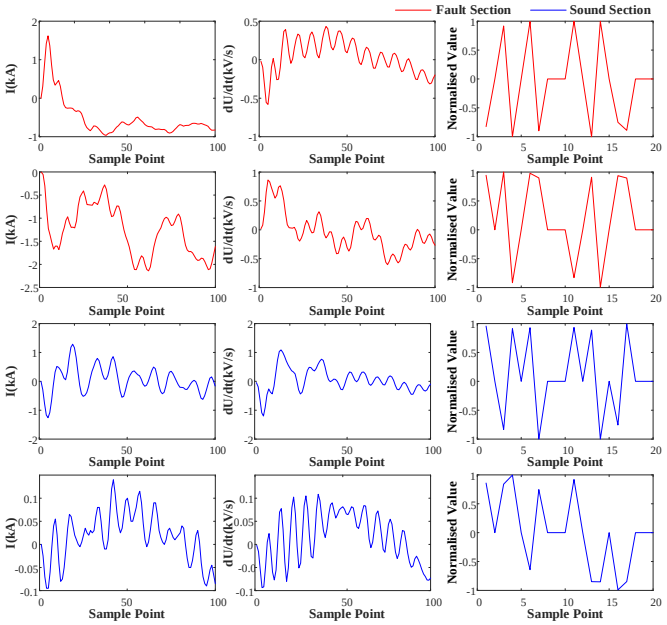

Fig. 12. TZSCs, DTZSVs, and spliced characteristic vectors of RTDS data.

TABLE V
PARAMETERS OF RTDS DATA

S_i	θ (degree)	R_f (ohm)	Quantity
S_1, S_2, S_5, S_6	30,45,60,90	10,100,1000	48

TABLE VI
TEST RESULTS OF PROPOSED METHOD WITH RTDS DATA

Training sample distribution	Number of training data	Number of test data	Accuracy
Nonuniformity	25	23	82.6%
Uniformity	20	28	96.4%

TABLE VII
TEST RESULTS OF RTDS DATA

Method	Accuracy	Precision	Recall	F_1-score
Proposed Method	96.4%	90.0%	100%	0.947
Method A	62.5%	52.0%	68.4%	0.591
Method B	64.3%	42.9%	33.3%	0.375

TABLE VIII
TEST RESULTS OF FIELD DATA

Method	Accuracy	Precision	Recall	F_1-score
Proposed Method	95.7%	83.3%	100%	0.909
Method A	62.2%	46.2%	37.5%	0.414
Method B	78.3%	0%	0%	0

E. Adaptability Analysis Based on Field Data

In a 10 kV substation in China, 11 groups of SPG fault data (45 sets in total) are collected in sampling frequency of 4 kHz. See Fig. 13 for the network structure of this substation, and 17 PSFISs are installed for detection. The data with 11 fault sections and 11 sound sections are selected for training while the remaining are used for testing. The TZSCs, DTZSVs, and spliced characteristic vectors of four sections are selected, as shown in Fig. 14.

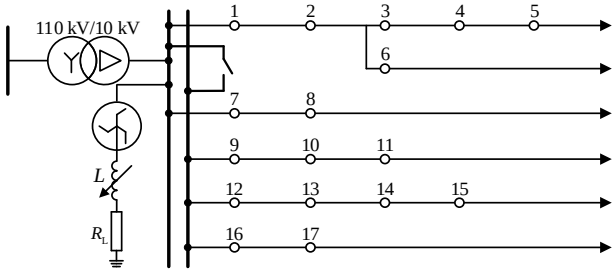

Fig. 13. Network structure of 10 kV substation.

As shown in Table VIII, the recognition rate of Method A is even worse than that of simulation, as FCM is susceptible to interferences and artificial extraction of fault features cannot guarantee to obtain all the essential features. As discussed in Section IV-B, the performance of 1-D CNN is deteriorated due to the discontinuity caused by directly splicing TZSC waveform and DTZSV waveform. Therefore, Method B has low reliability in industrial application. However, due to the adaptive feature extraction, the proposed approach still maintains a high accuracy of 95.7%, which indicates its high robustness and adaptability in case of the harsh field environment and irregular field data.

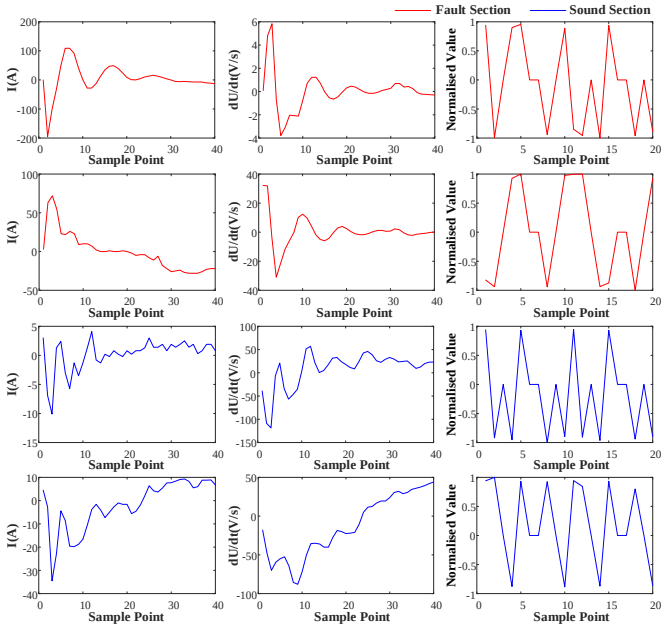

Fig. 14. TZSCs, DTZSVs, and spliced characteristic vectors of field data.

By analyzing the relationship between TZSC and DTZSV in each section, the proposed method can locate the fault section without relying on communication and analysis of the master station. In addition, the AE is adopted to extract the optimal features adaptively without training process, providing the proposed method a strong learning effect in case of small sample amount and harsh field environment. What is more, there is no need to manually set a threshold in the whole process.

Whilst the available field fault data is limited in this study, the excellent performance of the proposed method seen in the case studies shows a promising prospect of being implemented in real applications. However, it is still suggested to add new field fault data as available to the training set to enhance the coverage of training samples and conduct more comprehensive validation tests.

In the process of local intelligent research and judgment, the PSFISs of distribution systems will send their corresponding serial numbers and discriminant results to the master station for correctness check. The reidentification or manual inspections will be executed in case of misidentification to guarantee the accurate fault section isolation.

V. Conclusion

The deployment of the PSFIS brought new opportunities for locating the single phase to ground fault in resonant grounding distribution systems. The proposed decentralized fault section location method was to analyze the relation of TZSC and the DTZSV via AE, feature fusion, and backpropagation neural network. The simulation and experiment validation were expatiated and analyzed in details, which included simulation platform and model parameters, adaptability analysis based on the PSCAD/EMTDC simulation, adaptability analysis based on the real-time digital simulation data, and adaptability analysis based on the field data. The proposed method could provide a good performance in a wide range of fault scenarios in the case studies, indicating its high effectiveness and adaptability. In addition, the noise interference needs to be further considered in subsequent research.

Compared with the existing fault location methods, there were two main contributions of the proposed method.

1) The performance of existing methods were greatly affected by communication problems in practical applications. By using the waveform relation between TZSC and DTZSV in each section, the data could be analyzed locally at each PSFIS, which largely reduced the communication burden. And the local isolation capability of this method avoided the massive manpower consumption with improved reliability and efficiency.

2) The fault features were usually short and weak, methods that highly relied on artificially designed features showed poor robustness in industrial applications. In this article, the optimal features of fault data were adaptively extracted by AE without training process. The implementation of adaptive feature extraction and feature fusion greatly improved the adaptability of this method to factors like line type, network structure, fault resistance, compensation degree, sampling error, harsh field environment, and roughness of data.

References

[1] Y. Chen, J. Yin, Z. Li, and R. Wei, "Single-line-to-ground fault location in resonant grounded systems based on fault distortions," *IEEE Access*, vol. 9, pp. 34325–34337, Feb. 2021.

[2] D. Topolanek *et al.*, "Earth fault location based on evaluation of voltage sag at secondary side of medium voltage/low voltage transformers," *IET Gener., Transmiss. Distrib*, vol. 9, no. 14, pp. 2069–2077, Oct. 2015.

[3] J. Teng, W. Huang, and S. Luan, "Automatic and fast faulted line-section location method for distribution systems based on fault indicators," *IEEE Trans. Power Syst.*, vol. 29, no. 4, pp.1653–1662, Jul. 2014.

[4] K. Zhu, P. Zhang, W. Wang, and W. Xu, "Controlled closing of PT delta winding for identifying faulted lines," *IEEE Trans. Power Del.*, vol. 26, no. 1, pp. 79–86, Sep. 2011.

[5] L. Niu, G. Wu, and Z. Xu, "Single-phase fault line selection in distribution network based on signal injection method," *IEEE Access*, vol. 9, pp. 21567–21578, Jan. 2021.

[6] K. Sarwagya, S. De, and P. K. Nayak, "High-impedance fault detection in electrical power distribution systems using moving sum approach," *IET Sci., Meas. Technol.*, vol. 12, no. 1, pp. 1–8, Jan. 2018.

[7] B. Liu *et al.*, "Single-phase-to-ground fault detection with distributed parameters analysis in non-direct grounded systems," *CSEE J. Power Energy Syst.*, vol. 5, no. 1, pp. 139–147, Mar. 2019.

[8] M. Guo, X. Zeng, D. Chen, and N.-C. Yang, "Deep-learning-based earth fault detection using continuous wavelet transform and convolutional neural network in resonant grounding distribution systems," *IEEE Sens. J.*, vol. 18, no. 3, pp. 1291–1300, Feb. 2018.

[9] X. Wang *et al.*, "Location of single phase to ground faults in distribution networks based on synchronous transient energy analysis," *IEEE Trans. Smart Grid*, vol. 11, no. 1, pp. 774–785, Jan. 2020.

[10] N. Peng, R. Liang, G. Wang, P. Sun, C. Chen, and T. Hou, "Edge computing-based fault location in distribution networks by using asynchronous transient amplitudes at limited nodes," *IEEE Trans. Smart Grid*, vol. 12, no. 1, pp. 574–588, Jan. 2021.
[11] Y. Wang *et al.*, "Faulty feeder detection of single phase-earth fault using grey relation degree in resonant grounding system," *IEEE Trans. Power Del.*, vol. 32, no. 1, pp. 55–61, Feb. 2017.
[12] X. Wang, J. Gao, X. Wei, Z. Zeng, Y. Wei, and M. Kheshti, "Single line to ground fault detection in a non-effectively grounded distribution network," *IEEE Trans. Power Del.*, vol. 33, no. 6, pp. 3173–3186, Dec. 2018.
[13] Z. Wei, Y. Mao, Z. Yin, G. Sun, and H. Zang, "Fault detection based on the generalized S-transform with a variable factor for resonant grounding distribution networks," *IEEE Access*, vol. 8, pp. 91351–91367, May 2020.
[14] M. A. Barik, A. Gargoom, M. A. Mahmud, M. E. Haque, H. Al-Khalidi, and A. M. T. Oo, "A decentralized fault detection technique for detecting single phase to ground faults in power distribution systems with resonant grounding," *IEEE Trans. Power Del.*, vol. 33, no. 5, pp. 2462–2473, Oct. 2018.
[15] Y. Du *et al.*, "Single line-to-ground faulted line detection of distribution systems with resonant grounding based on feature Fusion Framework," *IEEE Trans. Power Del.*, vol. 34, no. 4, pp. 1766–1775, Aug. 2019.
[16] Y. Yu *et al.*, "Fault location in distribution system using convolutional neural network based on domain transformation," *CSEE J. Power Energy Syst.*, vol. 7, no. 3, pp. 472–484, May 2021.
[17] J. Gu, Z. Huang, J. Wang, L.-C. Hsu, and M.-T. Yang, "High impedance fault detection in overhead distribution feeders using a DSP-based feeder terminal unit," *IEEE Trans. Ind. Appl.*, vol. 57, no. 1, pp. 179–86, Oct. 2020.
[18] Q. Jia, X. Dong and S. Shi, "Practical traveling waves based single-phase-to-ground protection for radial connected distribution lines," *Proc. CSEE*, vol. 39, no. 6, pp. 1543–1550, Mar. 2019.
[19] W. Li, W. Chen, C. Guo, Y. Jin, and X. Gong, "Optimal placement of fault indicators in distribution system using PSO algorithm," in *Proc IECON-43rd Annu. Conf. IEEE Ind. Electron. Soc.*, 2017, pp. 375–380.
[20] L. Wen, L. Gao and X. Li, "A new deep transfer learning based on sparse auto-encoder for fault diagnosis," *IEEE Trans. Syst., Man, Cybern., Syst.*, vol. 49, no. 1, pp. 136–144, Jan. 2019.
[21] X. Xie, X. Li, D. Li, and L. Xu, "Real-time in-situ laser ranging via back propagation neural network on FPGA," *IEEE Sens. J.*, vol. 21, no. 4, pp. 4664–4673, Feb. 2021.
[22] H. Sun and Y. Xu, "Primary and secondary fusion technology of high reliability distribution network," *Trans. China Electrotech. Soc.*, vol. 1, pp. 1–2, Jan. 2020.
[23] L. He *et al.*, "Optimal placement method of fault indicator in distribution network considering reliability constraints," *Automat. Elect. Power Syst.*, vol. 44, no. 18, pp. 116–123, Sep. 2020.
[24] M. Farajollahi, M. Fotuhi-Firuzabad and A. Safdarian, "Simultaneous placement of fault indicator and sectionalizing switch in distribution networks," *IEEE Trans. Smart Grid*, vol. 10, no. 2, pp. 2278–2287, Mar. 2019.
[25] X. Shao, M. Guo and L. You, "Faulty line selection method using mutual correlation cluster of grounding fault waveforms based on improved DTW method," *Elect. Power Automat. Equip.*, vol. 38, no. 11, pp. 63–71, Nov. 2018.
[26] S. Zhuang *et al.*, "A line selection method for single-phase high-impedance grounding fault in resonant grounding system of distribution network based on improved euclidean-dynamic time warping distance," *Power Syst. Technol.*, vol. 44, no. 1, pp. 273–281, Jan. 2020.
[27] X. Wang *et al*., "High impedance fault detection method based on variational mode decomposition and Teager–Kaiser energy operators for distribution network," *IEEE Trans. Smart Grid*, vol. 10, no. 6, pp. 6041–6054, Nov. 2019.

Zi-Jing Li (Graduate Student Member, IEEE) was born in Zhangzhou, China, in 1997. She received the B.S. degree in 2019, in electrical engineering and automation from Fuzhou University, Fuzhou, China, where she is currently working toward the M.S. degree in electrical engineering.

Her research interests include power distribution systems and its automation, and application of artificial intelligence in power distribution systems.

Shuyue Lin received the B.Eng. degree (First Classis Hons.) in electrical power engineering from the University of Bath, Bath, U.K., in 2012, the second B.Eng. degree in electrical power engineering and automation from North China Electric Power University, China, in 2012, the M.Sc. degree (distinction) in control systems from Imperial College London, London, U.K., in 2013, and the Ph.D. degree in engineering from the University of Warwick, Conventry, U.K., in 2019.

She is currently a Lecturer with Fuzhou University, Fuzhou, China. She was an Electrical Engineer with Fujian Electric Power Survey and Design Institute, China. Her current research interests include the power generation and grid integration of the renewable energy.

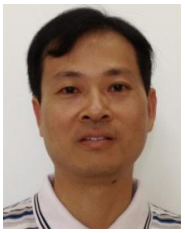

Mou-Fa Guo (Member, IEEE) was born in Fuzhou, China, in 1973. He received the B.S. and M.S. degrees from Fuzhou University, Fuzhou, China, in 1996 and 1999, respectively, and the Ph.D. degree from the Yuan Ze University, Taoyuan, Taiwan, in 2018, all in electrical engineering.

Since 2000, he has been a Professor with the College of Electrical Engineering and Automation, Fuzhou University, Fuzhou, China. His research interests include power distribution systems and its automation, and application of artificial intelligence in power distribution systems.

J, Tang was born in China in 1966. He received the M.S. degree in communication and electronic systems from Tsinghua University, Beijing, China, in 1991.

He is currently the Vice General Manager and Senior Engineer with Shanghai Holystar Information Technology Company, Ltd, Shanghai, China. His research interests include field application of distribution network equipment, online monitoring system of distribution feeder, GIS field of distribution systems, and wireless communication of distribution systems.